STM JOURNALS

Journal of
Geotechnical Engineering

ISSN: 2394-1987
Volume 9, Issue 1, 2022
DOI (Journal): 10.37591/JoGE

http://engineeringjournals.stmjournals.in/index.php/JoGE/index

Research JoGE

DEM Simulation of Macro and Micro-scale Behavior of Granular Materials during Loading and Unloading

Md. Mahmud Sazzad*

Abstract

The present paper aims at comparing the simulated stress-strain behavior of granular materials quantitatively with the experiment and exploring the evolution of the micro-scale behaviors during loading and unloading using the discrete element method (DEM). A numerical sample consisting of 9826 randomly generated spheres similar to the experiment was prepared. The numerically prepared isotropic sample was subjected to loading and unloading under strain controlled condition. It is noticed that the simulated stress-strain behavior agrees well with the experimental stress-strain behavior during loading and unloading. The evolution of micro-scale parameters is studied by varying the maximum applied strain. The evolution pattern of coordination number and slip coordination number depends on the maximum applied strain during loading and unloading. Slip coordination number evolves differently during loading from coordination number, but it evolves in a similar manner during unloading. The ratio of strong contacts to all contacts increases abruptly on reversal of loading, which is opposite to what is observed for coordination number and slip coordination number. The deviatoric fabric considering strong contacts mimics the deviatoric stress regardless of the values of maximum applied strain during loading and unloading. Fabric ratio can be linearly correlated to the stress ratio during loading and unloading regardless of the values of maximum applied strain when the contact normal vectors only at strong contacts are considered.

Keywords: Quantitative validation, Micro-scale quantities, Deviatoric fabric, DEM, Loading and Unloading.

INTRODUCTION

Granular material such as sand is often modeled with the continuum concept by using the finite element method (FEM). However, the models using the continuum concept are phenomenological and do not consider the fundamental physical processes of a particulate system. Fundamentally, the loads in a granular system are transferred by interparticle contacts. This inherent granulate nature of granular materials is not included in modeling the behavior of granular system in the continuum mechanics which cannot capture the actual deformation and failure modes of such system. The inherent discrete nature makes the development of constitutive laws very complex. Consequently, many physical tests are required to understand the behaviors at macroscopic scale before devolving a constitutive relation using the continuum concepts. Moreover, the inherent granulate behavior cannot be understood using the continuum approaches.

DEM, on the other hand, considers the fundamental physical processes of a granulate system and proves to be a useful tool in modelling the discrete nature of granular materials. The review of the earlier studies depicts that DEM is used extensively in most of the cases to simulate

***Author for Correspondence**
Md. Mahmud Sazzad

Professor, Department of Civil Engineering, Rajshahi University of Engineering & Technology, Rajshahi, Bangladesh

Received Date: March 03, 2022
Accepted Date: March 21, 2022
Published Date: March 30, 2022

Citation: Md. Mahmud Sazzad*. DEM Simulation of Macro and Micro-scale Behavior of Granular Materials during Loading and Unloading. Journal of Geotechnical Engineering. 2022; 9(1): 26–38p.

and explore the monotonic behavior of granular materials in two- and three-dimension [1–10]. However, a very few research works were presented in the literature that studied cyclic loading using the DEM [11–15]. For example, Ng and Dobry [11] studied the monotonic drained and undrained cyclic loading (constant volume) using the DEM and indicated that the simulated cyclic loading closely resembled the hysteresis loop formation and pore water pressure build up. Sazzad and Suzuki [13] studied the effect of inherent anisotropic conditions during cyclic loading using the 2D DEM models and indicated that the change in fabric anisotropy is dominant for the first few loading-unloading cycles. Considering the variation of the confining pressure in a 2D dry granular sample, Sazzad [14] studied the micro-scale behavior of granular materials during cyclic loading using the DEM. Kuhn et al. [15] investigated the cyclic liquefaction behavior using the DEM by considering the octahedral particles composed of the clusters of spheres. They proposed four scalar measures to predict the severity of a particular loading sequence and depicted that stress-based scalar measure exhibited the superior efficacy in predicting initial liquefaction and pore pressure rise. It should be noted that the aforementioned studies simulated the macromechanical behavior qualitatively using the DEM by applying the cyclic loading.

The qualitative comparison of the results obtained from the DEM simulation with the laboratory experiment is valid as long as the behavior of granular materials at the micro level is of the major interest or focus of the study. However, to authenticate the reliability of these micro-mechanical behaviors observed during the simulation and to have more confidence in the micro-mechanical responses using DEM, it is important that the simulated results by DEM are compared with the experimental results quantitatively and then, the evolution of different micro-mechanical parameters including fabric is explored. In spite of the fact, the quantitative validation of the DEM results with the experiment during the cyclic loading is rare in the literature. Among the earlier studies, only O'Sullivan et al. [12] reported a physical cyclic test using dry Grade chrome steel balls under vacuum confinement of 80 kPa and compared the experimental results with the DEM. Considering the limited number of such studies, it can be argued that more micro-scale mechanics should be studied to enhance our understanding during the cyclic loading. Thus, the first aim of this study is to compare the simulated stress-strain response during loading and unloading by DEM under strain controlled condition with that of the experiment reported in O'Sullivan et al. [12] quantitatively. After the quantitative comparison of the simulated stress-strain behavior during loading and unloading by DEM with the experiment, the evolution of different micro-scale parameters such as the coordination numbers and deviatoric fabric during loading and unloading is reported for different maximum applied strain. The fabric was quantified with the help of different fabric tensors. In this study, single micro-scale parameter is considered in contrast to many micro-scale parameters usually used in most other approaches in the literature to establish a macro-micro relation. The study depicts that a linear macro-micro relationship is possible considering a single micro-parameter during loading and unloading for different maximum applied strains.

ABOUT DEM AND OVAL

DEM was proposed by Cundall and Strack [16] for modeling the discrete nature of granular materials. The particles considered in DEM can translate and rotate independently through the interparticle contacts. The contacts between particles can even break. Newton's second law of motion is used to compute the translational acceleration and rotational accelerations of a 3D particle. The associated equations are as follows:

$$m\ddot{x}_i = \sum F_i \qquad i = 1-3 \tag{1}$$

$$I\ddot{\theta} = \sum M \tag{2}$$

where F_i stands for force components, M stands for moment, m stands for mass, I stands for the moment of inertia, $\ddot{x}_i$ stands for the translation acceleration components and $\ddot{\theta}$ stands for the rotational acceleration of the particle. The displacements of particles are obtained by integrating the accelerations twice over time. For the basic idea of DEM, readers are suggested to study the pioneering contributions by Cundall and Strack [16].

In the present study, computer program OVAL [2] is used. It is a program written in FORTRAN language and runs in both Windows and Linux platform. It is used for analyzing the particulate assemblies using DEM. It includes a robust servo-control algorithm to control the boundary stresses. OVAL has been recognized so far by many contributions in the literature and thus, its efficacy has been established [1, 8, 9, 17]. In the present study, Hertz-Mindlin contact model is used. The normal force of a Hertz-type contact is computed as follows [17]:

$$F^n = \frac{\overline{E}a^3}{R_e} \tag{3}$$

$$\overline{E} = \frac{8G}{3(1-\nu)} \tag{4}$$

$$a = \sqrt{\frac{d \times R_e}{2}} \tag{5}$$

$$R_e = \frac{2R_1R_2}{R_1 + R_2} \tag{6}$$

Here, $\overline{E}$ is the elastic constant, a is the contact radius, d is the overlap between the contacting particles, R_e is the effective radius of curvature, R_1 and R_2 are the radii of curvatures of two particles at contact.

BRIEF DESCRIPTION OF THE PHYSICAL CYCLIC TEST

In the present study, the cyclic shear test reported in O'Sullivan et al. [12] on dry grade chrome steel balls under a confinement of 80 kPa was simulated. The nonuniform sample in their study had three types of spheres having the radii of 2 mm, 2.5 mm and 3 mm, respectively. The mixing ratio of these spheres for nonuniform sample was 1:1:1. The height to width ratio and the void ratio of the sample were 2.0 and 0.603, respectively. The characteristics of the spheres used in the cyclic test as reported in O'Sullivan et al. [12] have been summarized in Table 1. The particle to particle friction coefficient and the boundary to particle friction coefficient were computed by O'Sullivan et al. [18] and Cui [19]. For details of the physical test, readers are referred to O'Sullivan et al. [12].

Table 1. Characteristics of dry Grade chrome steel balls used in the cyclic test [12].

Properties	Values
Density of spheres (kg/m^3)	7.8 ×10^3
Shear modulus (Pa)	7.9 ×10^3
Poisson's ratio	0.28
Interparticle friction coefficient	0.096
Boundary friction coefficient	0.228

Preparation of Numerical Sample

Sample Generation

Initially, a sparse sample was generated with 9826 spheres (radii of 2 mm, 2.5 mm and 3 mm) randomly in such a way that a sphere cannot touch its neighbors. The spheres were considered as particles because the physical test reported by O'Sullivan et al. [12] also considered dry grade chrome steel balls. The mixing ratio of these spheres was 1:1:1 similar to O'Sullivan et al. [12].

Preparation of Isotropically Compressed Sample

After the end of sample generation, the numerical sample was consolidated in different stages to attain the target confining pressure of 80 kPa similar to the physical test. During the isotropic compression, the periodic boundary condition was applied similar to that used in many other DEM based studies [1, 2]. A particle that sits astride a periodic boundary has a numerical image at the opposite boundary. If the centers of the particles move outside any boundary, they are instantly reintroduced at a corresponding position along the other boundary. The consolidation of the initially generated sparse sample was carried out using the strain controlled condition. When the isotropic compression was completed, the void ratio of the numerical sample became 0.626, which was very close to that reported in O'Sullivan et al. [12]. It should be noted that the void ratio of the isotropically consolidated numerical sample is a bit higher than that of the real sample. Such difference of the void ratio is believed to have negligible influence on the simulated results.

Numerical Simulation

The numerical sample was subjected to loading and unloading for different maximum applied strains ranging from 0.1% to 2% using the DEM. During loading, the sample height was decreased with a very small strain increment of 2.0×10^{-5} % per time step along the x_1 - direction by keeping the stresses in x_2 - direction and x_3 - direction constant (80 kPa). However, during unloading, the sample height was increased with the same strain increment along the x_1 - direction by keeping the stresses in x_2 - direction and x_3 - direction constant (80 kPa). The graphical illustration of the simulated model is depicted in Figure 1 for clarity.

A very small strain increment was assigned so that the quasi-static condition was attained and the effect of numerical damping became minimum. To monitor the quasi-static condition, a non-dimensional index I_{uf} is defined as follows [8]:

$$I_{uf} = \sqrt{\frac{\sum_{1}^{N_p} F_{ubf}^2 / N_p}{\sum_{1}^{N_c} F^2 / N_c}} \times 100\,(\%) \tag{7}$$

Here, F_{ubf} , F , N_c and N_p indicate the unbalanced force, contact force, number of contacts between particles and number of particles involved in the simulation, respectively. Index I_{uf} is directly related to the accuracy of the simulation. Lower the value of I_{uf} , higher the accuracy of the simulation. An average value of I_{uf} below 2% is observed during the simulation. The material properties and DEM parameters considered for the simulation of the present study are shown in Table 2. It can be observed that the material properties of spheres considered for the simulation of the present study are same as those of grade chrome steel balls used in the physical test (i.e. experiment).

Validation of Simulated Stress-strain Behavior with the Experiment

The simulated stress-strain behavior is compared with that of the physical cyclic test as reported in O'Sullivan et al. [12] and presented in Figure 2. The stress ratio is defined here as $R_\sigma = (\sigma_1 - \sigma_3)/\sigma_3$. Here, σ_1 indicates the stress in x_1 - direction and σ_3 indicates the stress in x_3 - direction. The simulated stress-strain behavior computed by the DEM during loading and unloading has excellent agreement with the physical test reported in O'Sullivan et al. [12] under the strain controlled condition. This quantitative validation of the simulated stress-strain behavior with that of the experiment during loading and unloading depicts the versatile nature of the present study by DEM. It proofs that DEM can successfully replicate the behavior of granular materials quantitatively. This quantitative validation of the numerical simulation by the DEM with the experiment during loading and unloading gives confidence about the authentication of the micro-scale responses reported in the following sections.

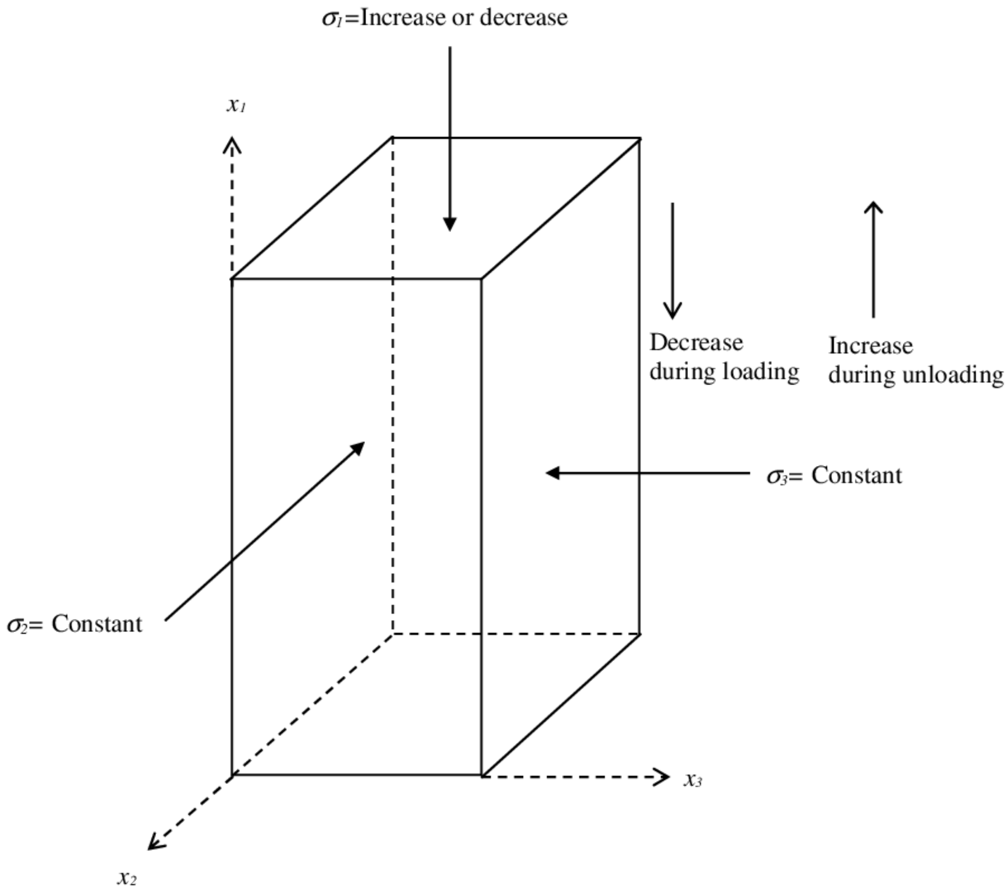

Figure 1. Graphical illustration of the simulated model with reference axes.

Table 2. Material properties and DEM parameters used in the present study.

Properties	**Values**
Density of spheres (kg/m^3)	7.8 ×10^3
Shear modulus (Pa)	7.9 ×10^3
Poisson's ratio	0.28
Interparticle friction coefficient	0.096
Increment of time step (s)	1.0 ×10^{-6}
Damping coefficients	0.10

Evolution of Micro-scale Behavior for Different Applied Strains

The evolution of micro-scale behavior such as the coordination number with axial strain is showed in Figure 3. The coordination number is conventionally defined as $Z = 2N_c / N_p$ [14].

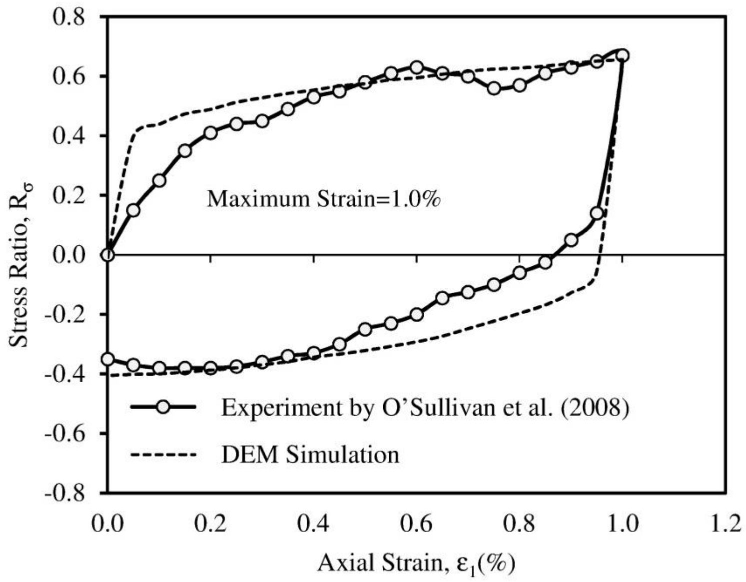

Figure 2. Comparison of the simulated stress-strain behavior with the experimental cyclic test reported by O'Sullivan et al. [12].

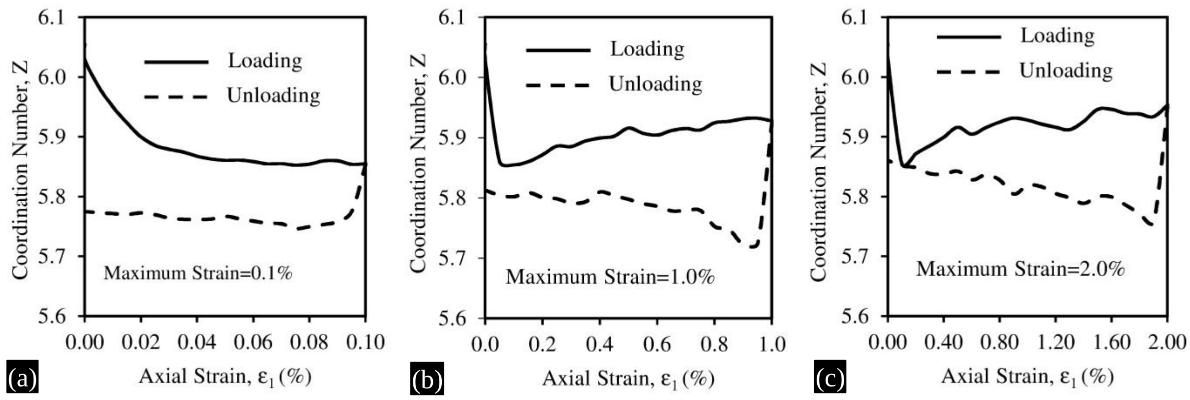

Figure 3. Evolution of coordination number with axial strain during loading and unloading for different values of maximum applied strain: (a) ε_1^{max}=0.10%, (b) ε_1^{max}=1.0%, (c) ε_1^{max}=2.0%.

In Figure 3, two sudden drops of coordination number are noticed. First drop is noticed when the isotropically compressed sample undergoes loading and second drop is noticed when the sample undergoes stress reversal (i.e. unloading). When the maximum applied strain ε_1^{max} is 0.10%, these drops are not as sharp as it is noticed in case when ε_1^{max}=1.0 % and ε_1^{max}=2.0%. When ε_1^{max} is 0.10%, the isotropically distributed contacts start to be lined with the major principal stress direction and few contacts are lost in the minor principal stress direction. As a result, the reduction of coordination number is not so sharp during loading. When the load is reversed, the principal stress direction is also reversed which leads to the disintegration of few more contacts resulting in a second drop of coordination number. For the case when ε_1^{max} is as large as 2.0%, the sample gets enough time to redistribute the isotropically distributed contacts prior to shear and the contacts are lined with the direction of major principal stress by losing huge contacts in the direction of minor principal stress. When the loading continues, the number of contacts and the coordination number starts increasing again to support the accumulated force chains almost parallel to the direction of major principal stress. Similar mechanism takes place during unloading. The coordination number starts increasing again after the sudden drop immediately after the load reversal.

The evolution of slip coordination number is showed in Figure 4. The slip coordination number is defined as $Z_{sl} = 2N_{sl} / N_p$ [14], where N_{sl} indicates the total slip contacts among particles in the sample at a given state. Slip coordination number keeps increasing, on an average, till the end of loading and experiences a huge drop when the load is reversed. The drop is due to the stress reversal to adjust the change in principal stress direction. The slip coordination number keeps increasing again as the unloading continues. It should be noted that the slip coordination number fluctuates significantly when $\varepsilon_1^{\max}$=2.0% both during loading and unloading.

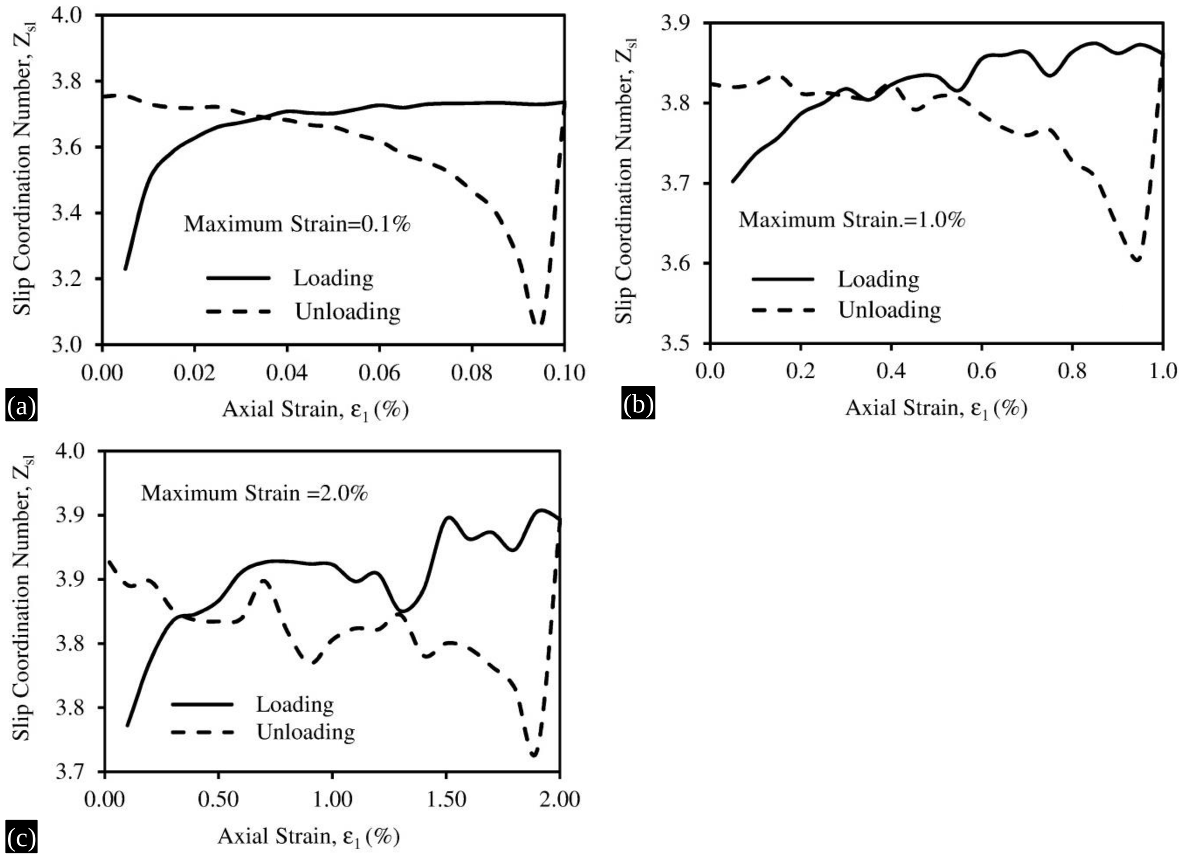

Figure 4. Evolution of slip coordination number with axial strain during loading and unloading for different values of maximum applied strain: (a) $\varepsilon_1^{\max}$=0.10%, (b) $\varepsilon_1^{\max}$=1.0%, (c) $\varepsilon_1^{\max}$=2.0%.

The development of deviatoric fabric $H_{11} - H_{33}$ with axial strain (ε_1) considering all contacts during loading and unloading for different applied strains is depicted in Figure 5(b). The fabric is usually characterized by contact normal vectors [20, 21]. The fabric considering all contacts can be quantified in term of the contact normal vectors as follows (Sazzad and Suzuki 2011, Sazzad 2014):

$$H_{ij} = \frac{1}{N_c} \sum_{\alpha=1}^{N_c} n_i^\alpha n_j^\alpha \qquad i, j = 1-3 \tag{8}$$

where n_i^α indicates the $i-$th component of the unit contact normal vector at the $\alpha-$th contact. A comparison of Figure 5(b) with Figure 5(a) shows that the evolution of deviatoric fabric with axial strain follows almost the same tendency of stress-strain curve during loading; however, the evolution of deviatoric fabric with axial strain deviates from the pattern (i.e. shape) of stress-strain curve during unloading.

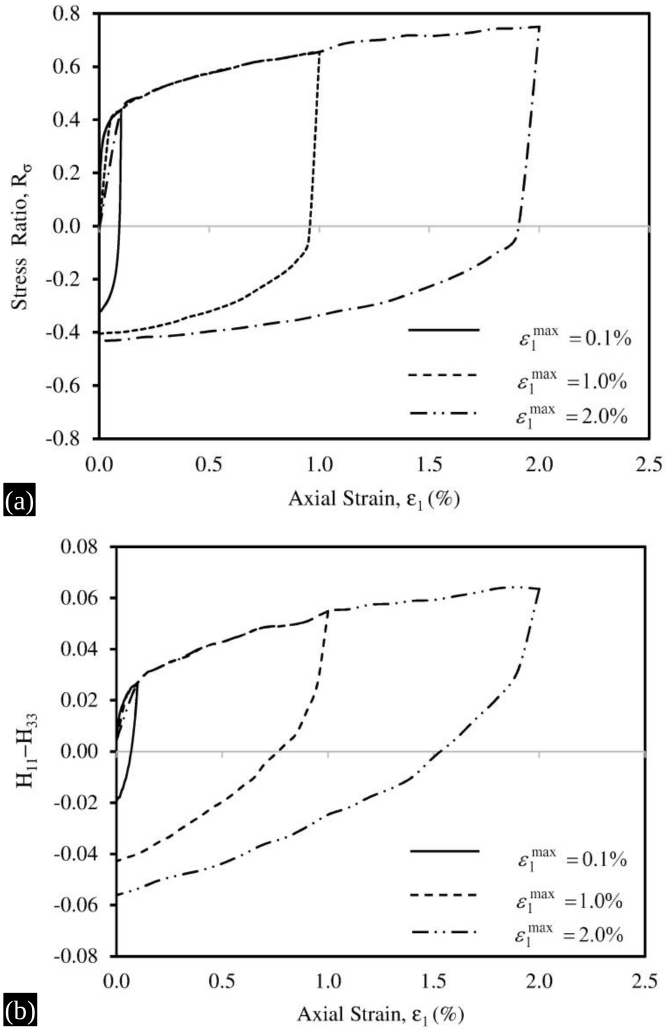

Figure 5. Evolution of (a) stress ratio and (b) deviatoric fabric considering all contacts with axial strain during loading and unloading for different values of maximum applied strain.

The fabric considering all contacts can be divided into two different fabrics: (i) strong contact fabric considering the contact normal vectors at strong contacts only and (ii) weak contact fabric considering the contact normal vectors at weak contacts only [8, 22]. In this study, a contact is said to be as a strong contact if the contact force (F) between the contacting particles is greater than the average contact force (F_a). Similarly, a contact is said to be as a weak contact if the contact force (F) between the contacting particles is smaller than or equal to the average contact force (F_a). The average contact force is delineated as follows:

$$F_a = \sqrt{\frac{\sum_{k=1}^{N_c} \left|F^k\right|^2}{N_c}} \tag{9}$$

where F^k indicates the contact force at the $k-$th contact. Before quantifying the strong contact fabric or weak contact fabric, the behavior of the ratio of strong contacts to the total contacts R can be examined. The evolution of R with axial strain during loading and unloading is portrayed in Figure 6. The ratio of strong contacts to the total contacts decreases gradually except when ε_1^{max} is

0.10%. Although the coordination number starts increasing after an initial reshuffle as loading continues (Figure 3), R on the contrary, keeps decreasing as one can notice in Figure 6. Although R reduces, the stress ratio at the same state of stress does not reduces (please note Figure 5(a)), because these contacts carry larger stress at these states. R jumps up again immediate after the load reversal due to the sudden change of the principal stress direction. Later, R keeps reducing, on an average, during unloading similar to the loading.

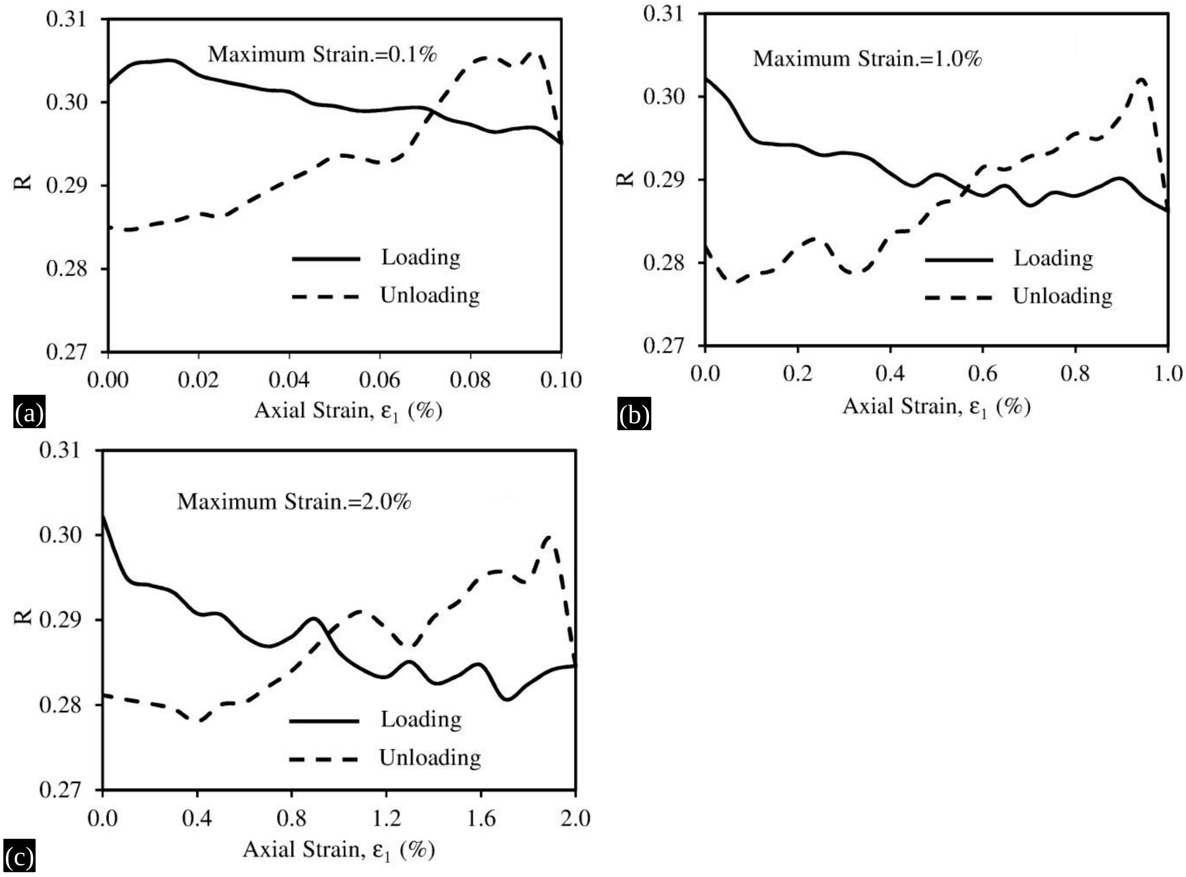

Figure 6. Evolution of R with axial strain during loading and unloading for different values of maximum applied strain: (a) $\varepsilon_1^{\max}$=0.10%, (b) $\varepsilon_1^{\max}$=1.0%, (c) $\varepsilon_1^{\max}$=2.0%.

Since strong contacts have significant role in the evolution of micro-structures [14, 17], the strong contact fabric tensor is defined similar to Eq. (8) as follows [8]:

$$H_{ij}^{s} = \frac{1}{N_c}\sum_{s=1}^{N_s} n_i^s n_j^s \qquad i, j = 1-3 \tag{10}$$

where n_i^s denotes the $i-$th component of the unit contact normal vector at the $s-$th strong contact and N_s denotes the total number of strong contacts.

The behavior of the deviatoric fabric $H_{11}^s - H_{33}^s$ for different applied strains with axial strain (ε_1) during loading and unloading is showed in Figure 7. It is noticed that the qualitative pattern of the evolution of fabric considering strong contacts is closer to the stress-strain curve during loading and unloading compared to the evolution of fabric considering all contacts. Since the evolution of $H_{11}^s - H_{33}^s$ with axial strain is similar to that of stress ratio with axial strain, it is intended to compare these results quantitatively. For this, the deviatoric fabric for strong contacts is divided by H_{33}^{s} similar to stress ratio and shown in Figure 8. It is evident from Figure 8 that fabric ratio [$(H_{11}^{s} - H_{33}^{s})/H_{33}^{s}$] quantified by a fabric tensor of contact normal vectors at strong contacts can replicate the stress-strain behavior of granular material during loading and unloading. This establishes an excellent linkage between the macro quantity (stress ratio) and the micro quantity (fabric ratio considering strong contacts). Please note, however that some mismatch between the simulated and experiment data in Figures 1 and 8 is observed. This may be due to the difference in the boundary conditions in the simulation and experiment. The present simulation considers the periodic boundary whereas the experiments used the flexible boundary.

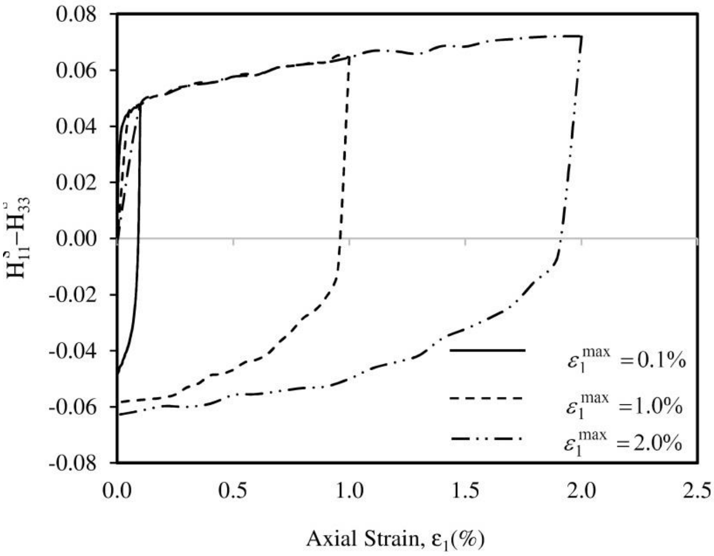

Figure 7. Evolution of deviatoric fabric considering contact normal vectors at strong contacts with axial strain during loading and unloading for different values of maximum applied strain.

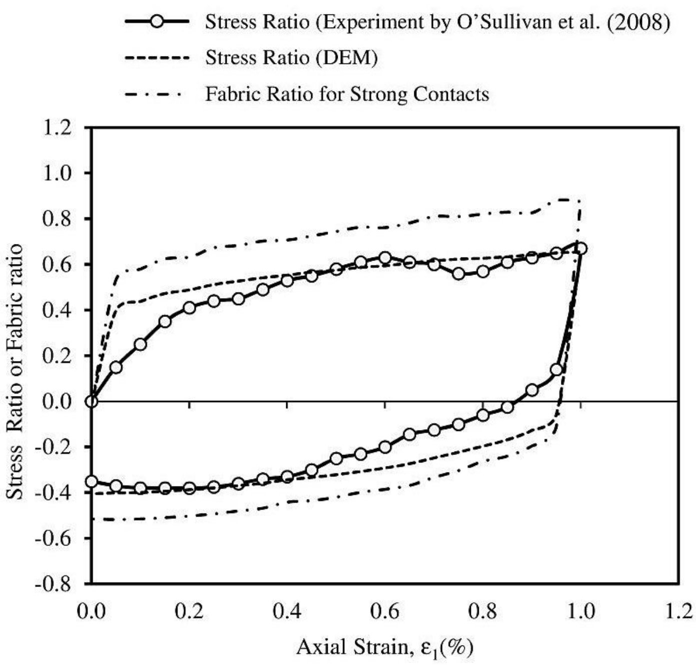

Figure 8. Comparison of the simulated stress ratio and fabric ratio with the evolution stress ratio during the experimental cyclic test.

Since an excellent linkage between the stress ratio and the fabric ratio considering strong contacts is noticed, a relationship between them can be established. In the literature, the relationship between the macro quantity such as the stress ratio and micro quantities regarding contact normal vectors, normal stress and tangential stress was noticed. For example, in several studies, the relationship between the stress ratio and the anisotropies initiated from the contact normal vector, normal contact force and tangential contact force is established [23–26]. In contrast to such approach, in this study, an attempt is made to correlate the stress ratio with the fabric ratio computed from the contact normal vectors of strong contacts [13]. In this approach, only single micro-scale parameter related to the contact normal vectors is used and thus, this approach is simpler compared to the most other approaches in the literature. Figure 9 represents the correlation between the fabric ratio for strong contacts and stress ratio.

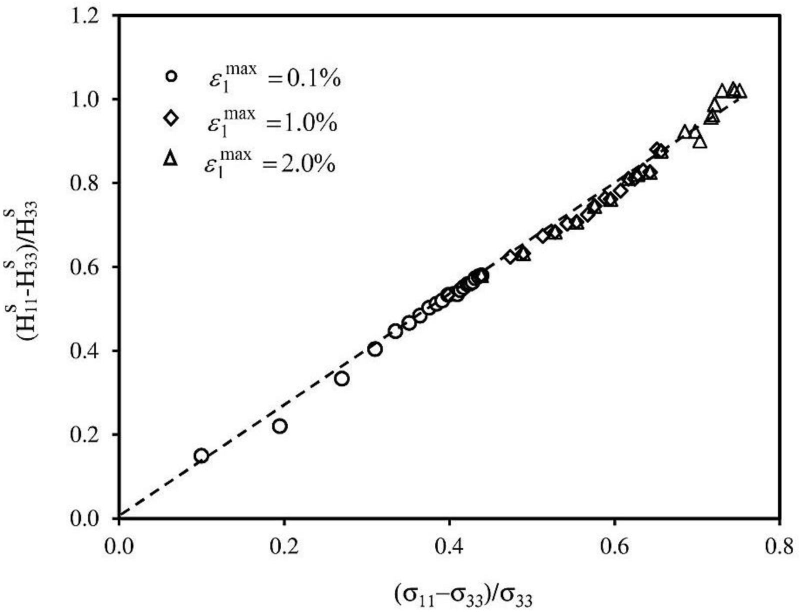

Figure 9. The relationship between the micro-quantity (fabric ratio) and macro-quantity (stress ratio) during loading and unloading for different values of maximum applied strain.

Interestingly, a linear correlation between the macro and micro quantity exists regardless of the maximum applied strain during loading and unloading. The correlation between the micro-quantity (fabric ratio) and macro-quantity (stress ratio) can be expressed as follows:

$$\left(\frac{H_{11}^s - H_{33}^s}{H_{33}^s}\right) = 1.32\left(\frac{\sigma_{11} - \sigma_{33}}{\sigma_{33}}\right) \tag{11}$$

CONCLUSIONS

In this study, the simulated stress-strain response during loading and unloading using the DEM is compared quantitatively with that of the experiment. In addition, the micro-mechanical responses during loading and unloading are explored for different applied strains. The evolution of fabric during loading and unloading is described and quantified using the fabric tensors considering all and strong contacts. The major findings of the present study are presented as follows:

1. The simulated drained cyclic behavior displays the similar stress-strain behavior as reported in the experiment except the initial stiffness of the stress-strain curve during loading.
2. The evolution pattern of coordination number as well as slip coordination number is a function of the maximum applied strain during loading and unloading. Slip coordination number evolves

differently during loading from coordination number but it evolves in a similar pattern during unloading.

3. The ratio of strong contacts to all contacts increases abruptly as soon as the load is reversed which is opposite to the behavior of coordination number and slip coordination number.
4. The deviatoric fabric considering strong contacts mimics the deviatoric stress regardless of the maximum applied strain during loading and unloading.
5. Fabric ratio can be linearly correlated to the stress ratio during loading and unloading considering the contact normal vectors at strong contacts. This approach of correlating the fabric defined by using a single parameter related to contact normal vectors at the strong contacts is simpler compared to the most other approaches in the literature.

REFERENCES

1. Azéma, E., Radjai, F., Peyroux, R., and Saussine, G. (2007). Force transmission in a packing of pentagonal particles. Physical Review E, 76 (1), 01130. DOI: 10.1103/PhysRevE.76.011301.
2. Azéma, E., Radjai, F., and Saussine, G. (2009). Quasistatic rheology, force transmission and fabric properties of a packing of irregular polyhedral particles. Mechanics of Materials, 41(6), 729-741. DOI: 10.1016/j.mechmat.2009.01.021.
3. Cui, L. (2006). Developing a virtual test environment for granular materials using discrete element modeling. PhD Thesis, University College Dublin, Ireland.
4. Cui, L., O'Sullivan, C., and O'Neil, S. (2007). An analysis of the triaxial apparatus using a mixed boundary three-dimensional discrete element model." Geotechnique, 57(10), 831–844, DOI: 10.1680/geot.2007.57.10.831.
5. Cundall, PA., and Strack, ODL. (1979). A discrete numerical model for granular assemblies. Geotechnique, 29(1), 47-65. DOI: 10.1680/geot.1979.29.1.47.
6. Jiang, MJ., Yu, H-S., and Harris, D. (2005). A novel discrete model for granular material incorporating rolling resistance. Computers and Geotechnics, 32(5), 240-357, DOI: 10.1016/j.compgeo.2005.05.001.
7. Kuhn, MR. (1999). Structured deformation in granular materials. Mechanics of Materials, 31(6), 407-429. DOI: 10.1016/S0167-6636(99)00010-1.
8. Kuhn, MR. (2003). Smooth convex three-dimensional particle for the discrete element method. Journal of Engineering Mechanics, 129(5), 539-547. DOI: 10.1061/(ASCE)0733-9399(2003)129:5(539).
9. Kuhn, MR., Renken, HE., Mixsell, AD., and Kramer, SL. (2014). Investigation of cyclic liquefaction with discrete element simulations. Journal of Geotechnical and Geoenvironmental Engineering, 140(12), 1-13. DOI: 10.1061/(ASCE)GT.1943-5606.0001181.
10. Ng, T-T. (2001). Fabric evolution of ellipsoidal arrays with different particle shapes. Journal of Engineering Mechanics, 127(10), 994-999, DOI: 10.1061/(ASCE)0733-9399(2001)127:10(994).
11. Ng, T-T., and Dobry, R. (1994). Numerical simulations of monotonic and cyclic loading of granular soil. Journal of Geotechnical Engineering, 120(2), 388-403. DOI: 10.1061/(ASCE)0733-9410(1994)120:2(388).
12. Nouguier-Lehon, C., Cambou, B., Vincens, E. (2003). "Influence of particle shape and angularity on the behavior of granular materials: a numerical analysis." International Journal of Numerical Analytical Methods in Geomechanics, 27(14), 1207-1226. DOI: 10.1002/nag.314.
13. Oda, M., Nemat-Nasser, S., and Konishi, J. (1985). Stress-induced anisotropy in granular masses. Soils and Foundations, 25(3), 85-97. DOI: 10.3208/sandf1972.25.3_85.
14. O'Sullivan, C., Bray, J., and Riemer, M. (2004). An examination of the response of regularly packed specimens of spherical particles using physical tests and discrete element simulations. Journal of Engineering Mechanics, 130(10), 1140–1150. DOI: 10.1061/(ASCE)0733-9399(2004)130:10(1140).
15. O'Sullivan, C., Cui, L. and O'Neill, SC. (2008). Discrete element analysis of the response of granular materials during cyclic loading. Soils and Foundations, 48(4), 511-530, DOI: 10.3208/sandf.48.511.

16. Ouadfel, H., and Rothenburg, L. (2001). Stress-force-fabric relationship for assemblies of ellipsoids. Mechanics of Materials, 33(4), 201–221. DOI: 10.1016/S0167-6636(00)00057-0.
17. Radjai, F., Wolf, DE., Jean, M., and Moreau, JJ. (1998). Bimodal character of stress transmission in granular packings. Physical Review Letter, 80(1), 61–64. DOI: 10.1103/PhysRevLett.80.61.
18. Rothenburg, L., and Bathurst, RJ. (1989). Analytical study of induced anisotropy in idealized granular materials. Geotechnique, 39(4), DOI: 601–614, DOI: 10.1680/geot.1989.39.4.601.
19. Sazzad, MM., and Suzuki, K. (2010). Micromechanical behavior of granular materials with inherent anisotropy under cyclic loading using 2D DEM., Granular Matter, 12(6), 597–605, DOI: 10.1007/s10035-010-0200-0.
20. Sazzad, M., and Suzuki, K. (2011). Effect of interparticle friction on the cyclic behavior of granular materials using 2D DEM. Journal of Geotechnical and Geoenvironmental Engineering, 137(5), 545-549. DOI: 10.1061/(ASCE)GT.1943-5606.0000441.
21. Sazzad, MM. (2014). Micro-scale behavior of granular materials during cyclic loading. Particuology, 16, 132-141. DOI: 10.1016/j.partic.2013.12.005.
22. Sazzad, MM., Sayera, K., Shaha, RK., and Islam, MS. (2015). “Macro and micro responses of granular materials under plane strain compression by 3D DEM.”, International Journal of Advanced Structures and Geotechnical Engineering, 4(2), 114-119.
23. Sazzad, MM. (2016). Micro-scale responses of granular materials at different confining pressures using DEM. Acta Geotechnica. Slovenica, 13(1), 26-36.
24. Sazzad, MM., Sneha, E., and Rouf, RB. (2017). Comparison of stress-stain behavior of CTC test using DEM simulation. International Conference on Planning, Architecture and Civil Engineering, Bangladesh, pp. 194-199.
25. Sazzad, MM (2019) Effect of intermediate principal stress on the behavior of granular materials at a low mean stress by DEM. Geotechnical and Geological Engineering, 37(5), DOI: 4539–4550. DOI: 10.1007/s10706-019-00929-7
26. Yang, Y., Fei, W., Yu., H-S., Ooi, J., and Rotter, M. (2015). Experimental study of anisotropy and non-coaxiality of granular solids, Granular Matter, 17(2), 189–196. DOI: 10.1007/s10035-015-0551-7.

